A Genome-wide CRISPR screen unveils the endosomal maturation protein WDR91 as a promoter of productive ASO activity in melanoma

Grégory Menchon[1], Aris Gaci[2], Antti Matvere[1], Marc Aubry[1], Aurélien Bore[3], Aurélie Goyenvalle[2] and Rémy Pedeux[1*]

[1] INSERM, OSS, UMR_S 1242, Univ. Rennes, 35000, Rennes, France

[2] Université Paris-Saclay, UVSQ, Inserm, END-ICAP, 78000 Versailles, France

[3] CRISPR'iT Genetic Platform Screening, Institut Curie, INSERM U934, CNRS UMR3215, 75005, Paris, France

*Corresponding author. Email: remy.pedeux@univ-rennes.fr

SHORT TITLE

A CRISPR screen unveils protein modulators of ASO activity

ABSTRACT

Antisense oligonucleotides (ASOs) belong to promising therapeutic molecules for the treatment of neurologic, muscular and metabolic disorders. Several ASOs have been approved so far and more than a hundred clinical trials are currently underway covering a dozen therapeutic areas including cancer. Yet, the mechanisms of internalization, cell trafficking and action of these molecules remain poorly understood. Moreover, with only a small fraction of ASOs reaching the correct cellular compartment following systemic delivery, the majority of targeted diseases

requires recurrent injections of ASOs. A deeper understanding of these mechanisms would guide the improvement of their potency and thus, reduce the amount of delivered ASOs and their potential side-effects. Here, using a CRISPR screen, we investigated intracellular proteins involved in ASOs efficiency using a whole genome approach and identified several potential regulators which could significantly impact ASOs potency in melanoma cells. From these proteins, we validated WD Repeat Domain 91 (WDR91), a regulator of endosomal maturation, as a modulator whose depletion significantly inhibits ASO productive activity. This study provides the first list of ASO modulators using a biologically relevant functional assay to estimate the role of these proteins. In conclusion, these data could lead to a better understanding of the mechanisms favoring productive uptake or improved endosomal escape of ASOs.

INTRODUCTION

Antisense Synthetic Oligonucleotides (ASOs) belong to a class of attractive therapeutic compounds for numerous diseases. ASOs modulate cellular target gene expression through Watson-Crick binding to complementary RNA molecules and, according to their type, act by either promoting a RNAse-H1 mediated RNA degradation (Gapmers - GMs) or through a steric blocking mechanism (mixmers and target site blockers – TSBs) leading to three major modes of action: inhibition or activation of gene-expression and splicing modulation[1]. ASOs have been developed for the treatment of different genetic disorders and they can be translated to personalized therapies[2]. ASOs are specially taken up by fast growing cells[3] and, among numerous advantages, bypass the current bottleneck regarding the targets that are considered undruggable with traditional small molecule inhibitors[4]. Several ASOs are currently approved by the Food and Drug Administration (FDA) for genetic and rare diseases[5,6] and several phase II and III studies are ongoing in the oncology therapeutic area[7].

46 Although ASOs promise a great leap forward in future cancer treatments, their utilization
47 suffers from major hurdles. Among them, a lack of tissue specific targeting[8,9] , poor cellular
48 uptake[10] and the need to escape from the endo-lysosomal pathway to exert their role in either
49 the cytoplasm or nucleus of the cells[11,12]. Moreover, the mechanisms of internalization, cell
50 trafficking and action of these molecules remain poorly understood. A small fraction of ASO
51 reaching the right cellular compartment and target following systemic delivery[13,14] leads to
52 treatments consisting of high doses, recurrent injections and thus, significant accumulation in
53 other non-targeted cells and organs with consecutive toxicities[15]. It is therefore essential to
54 better understand the fate of internalized ASOs and their intracellular route and mode of action.
55 Such deeper characterization in different cell lines and with different ASO types and
56 chemistries would help in the rational design and improvement of therapeutic ASO strategies
57 in future clinical applications. Several studies have demonstrated that the fate of internalized
58 phosphorothioate (PS)-containing ASOs was determined by intracellular interacting
59 proteins[16,17,18]. Even if a clear mechanism is still to be fully understood, around 80 intracellular
60 proteins have been identified and this protein interactome appears to influence the
61 pharmacological activities and potential toxicities of PS-ASOs by acting on their uptake and
62 distribution. It is also worth noting that many other proteins that bind to ASOs have no effect
63 on their activity. PS-ASOs are internalized and processed through the endocytic pathway[3,19],
64 but proteins can modulate endosome traffic and maturation without interacting directly with
65 oligonucleotides. Previous studies have investigated the modulation of intracellular pathways
66 to increase the productive delivery and activity of oligonucleotides and to further unveil the
67 critical molecular factors that contribute to nucleic acids pharmacological effects[20]. Among
68 these, modulation of endocytic recycling[21,22], multivesicular bodies' (MVBs) fusion with
69 lysosomes[23], endosomal escape[24] and nuclear shuttling[25,26] were explored. All these strategies
70 involve the use of either genetic or non-genetic perturbations and have proven to be successful

71 in many *in vitro* and *in vivo* studies. ASO-interacting proteins have been mostly characterized
72 by *in vitro* studies using pull-down experiments on cell lysates[27,28] but such method lacks
73 physiological relevance as the intracellular membrane's integrity is not preserved and could
74 lead to many binding artefacts. Furthermore, pull-down studies may highlight some important
75 ASOs protein modulators but only allow the identification of direct interactants. To circumvent
76 these issues other authors recently used proximity biotinylation assay to highlight
77 oligonucleotides interactome in living cells and in pharmacologically relevant conditions[29].

78 Clustered Regularly Interspaced Short Palindromic Repeats (CRISPR) screen is a powerful
79 genetic perturbation method that can be used for functional genomic studies, by activating or
80 silencing genes[30]. Then, it can be implemented to identify ASOs direct and indirect modulators
81 in a more physiological state and preserving the cell membrane's integrity. This technique was
82 implemented in different studies to investigate modulators of dsRNAs[31], Antibody-Drug
83 Conjugates (ADCs)[32] or encapsulated mRNAs[33], but to our knowledge, only one study
84 describes such a functional genomic screen (CRISPR gene activation) to uncover factors
85 enhancing ASOs activity[34].

86 In the present work, we used a genome-wide CRISPR screen strategy (CRISPR knockout), to
87 uncover proteins that modulate the potency of an anti-proliferative tricyclo-DNA (tcDNA)
88 based-ASO in a melanoma cell line (501Mel). The generation of the parental knockout cell
89 library was performed such as every single cell had a unique depleted coding gene. The library
90 was then treated with ASO, and sequencing was performed on the surviving (enriched or
91 depleted) cells. This analysis highlighted several candidates of interest (95 activators and 55
92 inhibitors). From the top candidates, the robustness of our assay also allowed to highlight the
93 proteins Ras-related protein Rab5C (Rab5C) and Component of Oligomeric Golgi Complex 8
94 (COG8) which are known positive regulators of ASOs productive trafficking and activity[35,36].

95 We unveiled the endosomal maturation protein WDR91 as a strong positive regulator of the
96 tcDNA based-ASO activity in this cell line. Activity modulation by WDR91 was validated
97 together with Annexin A2 (ANXA2), a well characterized endosomal protein which promotes
98 ASOs trafficking and productive activity in different cell lines[37]. The impact of WDR91 was
99 not validated on a splice switching ASO in a muscle cell line, highlighting a cell type-dependent
100 effect. Finally, this work provides a detailed source of potential positive and negative regulators
101 of ASO activity, coming from an unbiased screen and with a strong physiological relevance.

102

103 RESULTS

104 **Development and *in vitro* validation of a tcDNA-ASO to inhibit 501Mel cells proliferation**
105 **with a target-site blocking mechanism**

106 Previous work aiming at masking a microRNA (miRNA) target site on a microRNA sponge
107 (*TYRP1* mRNA) led to the test and validation of a commercially-designed Locked Nucleic Acid
108 (LNA) TSB (named TSB-T3 for Target-Site Blocking – T3). In this study, TSB-T3 significantly
109 induced the reduction of melanoma tumor growth *in vitro* and in 501Mel xenografts[38]. This
110 ASO was validated in five different cell lines and had a dose-response anti-proliferative
111 activity. TSB-T3 exerts its ASO masking activity by preventing the sequestration of the miR-
112 16 tumor suppressor by *TYRP1* mRNA and redirecting it towards its target-RNAs, to induce
113 their decay and subsequently reduce tumor proliferation[39] (Figure 1A). This miRNA
114 displacement mediated by a Target Site Blocker ASO represents a relevant assay to investigate
115 the proteins involved in ASOs efficiency. The ASO blocking activity is directly monitored
116 through an anti-proliferative effect, which has been validated *in vivo*.

117 In the present study, we decided to look for protein modulators of an ASO with a clinically
118 relevant chemistry. We thus designed and evaluated a new TSB-T3 with the same sequence but

119 with a full tcDNA chemistry and phosphorothioate (PS) backbone (tcT3). This class of
120 conformationally constrained ASO displays enhanced binding properties to DNA and RNA as
121 well as unique pharmacological properties and unprecedented uptake by many tissues after
122 systemic administration[40,41].

123 To compare both chemistries, 501Mel cells were reverse-transfected in 96-well plates with
124 either the LNA- or the tcDNA-ASO (named respectively T3 and tcT3). We deliberately used
125 high doses of ASOs (up to 70nM) as their blocking activity is based on the displacement of a
126 sequestered miR-16 by *TYRP1* mRNA which is, besides, highly expressed in melanoma cells
127 (with around 3200 copies per cell)[38]. After 72h, the cell density was measured by colorimetric
128 assay and normalized to a control ASO treatment (C1 or tcC1). As expected, we confirmed
129 previous results with the commercial reagent. Both T3 and tcT3 ASOs showed a dose-response
130 anti-proliferative activity and, interestingly, the tcDNA chemistry improved the ASO potency
131 at low doses (Figure 1B). This tcDNA-ASO was selected for the subsequent screening
132 experiment.

133

134 **Genome-wide pooled sgRNA library generation, knockout library treatment with tcDNA-**
135 **ASOs and NGS sequencing**

136 The CRISPR-knockout cell library was generated by transducing 501Mel cells with a pooled
137 lentiviral library which contains the Cas9 and sgRNAs targeting 19.114 human coding genes.
138 This lentivirus library contains 4 different guides per coding gene (total of 76.441 sgRNAs) and
139 1000 non-targeting control sgRNAs. A multiplicity of infection (MOI) of 0.4 was selected to
140 ensure that only few cells are transduced with more than one sgRNA and avoid unspecific
141 screening results[42]. With 76.441 sgRNAs and a desired coverage of at least 400 cells per guide,
142 a total of 32 million cells have been transduced and maintained during the screen.

143 After transduction, the cells were positively selected with antibiotic, expanded and
144 subsequently transfected with either the tcT3 or -C1 ASOs. A final ASO concentration of 50nM
145 was selected based on the former dose-response experiment which showed that the anti-
146 proliferative effect reached a plateau at this dose (Figure 1B). The treatment was performed for
147 three days. After this period, the difference in cell density between the treated and control
148 conditions was greater than 50%.

149 At the end of treatment, the cells were expanded, pooled and a pellet of 100 million cells per
150 condition was used for genomic DNA (gDNA) extraction and PCR amplification of the
151 integrated sgRNAs in the 3 conditions (non-treated parental cell bank, tcT3 treated and tcC1
152 treated). The global workflow is depicted in Figure 2A.

153 After amplicons sequencing by NGS, a quality check was performed and only 115 sgRNAs
154 were not detected over 76.441 in our cell library (0.15%), which validated proper conditions
155 before ASOs treatment. The normalized reads count in each control and therapeutic ASO
156 condition were plotted and provided a mean of 400-500 reads per guide as expected (Figure
157 2B).

158 The sequenced sgRNAs coming from the pool of surviving cells after ASO treatment provided
159 information regarding the enriched or depleted ones. Thus, by comparing the sgRNAs
160 enrichment or depletion in treated *versus* control condition and for each gene, we sought to
161 identify proteins potentially involved in the regulation of ASO uptake, trafficking, release and
162 guidance to their RNA-target in this melanoma cell line (Figure 2C).

163

164 **Identification of tcT3 ASO activity regulators in 501Mel cells**

165 To identify proteins that could impact the tcT3 activity in 501Mel cell line, the NGS sequencing
166 raw data accounting for the total number of sgRNA reads per gene and per sample were

167 analyzed as follows. First, we used MAGeCK count to collect sgRNA read count information
168 from the tcC1- and tcT3-treated cells sequencing files. Then, we used MA Plots to score and
169 identify candidates based on the sgRNA read abundance (A value) and the read counts ratio
170 between the treated and the control condition (M value: fold change - FC). M and A values
171 were computed for each of the 4 sgRNAs targeting each individual gene (Figure 3A). From the
172 MA plots, top activator and inhibitor candidates were extracted after using a defined M cutoff
173 for each sgRNA per gene. The figure 3B represents MA plot examples from selected activator
174 and inhibitor candidates with applied M cutoff and with 4 (GGTLC2) or 2 relevant sgRNAs
175 (WDR91). Because of a short time of treatment (72h), a minimum FC of 1.5 was fixed between
176 the tcT3 and tcC1 read counts to highlight the best hits (activator candidates: fold change tcT3
177 read counts *vs* tcC1 read counts ≥ 1.5; inhibitor candidates: fold change tcC1 read counts *vs*
178 tcT3 read counts ≥ 1.5) (Candidates examples in Figure 3C). We opted for a short time of
179 treatment to avoid guide selection bias.

180 Several sgRNAs targeting the same gene might not have a consistent behavior. However, the
181 Brunello library has been designed with optimized sgRNAs and is known to outperform other
182 knockout libraries[43]. Indeed, the robustness of this library has already been demonstrated with
183 the ability to identify reliable candidates with only 2 effective sgRNAs per gene[43]. We thus
184 extracted activator and inhibitor candidates considering two, three or four out of four guides
185 meeting the defined M (FC) and A selection criteria.

186 As shown in Figure 4A and B (and in supplementary Table 1), this cutoff allowed to highlight
187 a set of 95 activator candidates and 55 inhibitors. Regarding the activators, 5 genes had their 4
188 respective sgRNAs fulfilling the corresponding criteria; 28 genes had 3 effective sgRNAs and
189 62 genes had 2 effective sgRNAs over 4. From the inhibitors, 3, 7 and 45 genes had 4, 3 and 2
190 effective sgRNAs, respectively. Each of the candidates have been represented by an average

191 FC value but a detailed table of each sgRNA and their respective M, A and FC values is
192 available in supplementary Table 1.

193 Gene set enrichment analysis using PANGEA (Pathway, Network and Gene-set Enrichment
194 Analysis) allowed to classify the activator and inhibitor candidates based on the cellular
195 component gene ontology[44] (Supplementary Figures 1 and 2). Interestingly, the activator
196 candidates with the highest fold enrichment are mainly clustered within proteins belonging to
197 the peroxisome and mitochondria compartments. Inhibitor candidates are mainly clustered
198 within proteins belonging to the Golgi apparatus and microtubules regulation.

199 For subsequent validation experiments, we decided to focus on protein activators of ASOs since
200 we were more interested in the mechanistic uptake and trafficking of ASOs in cells. From the
201 list of activators having 3 effective sgRNAs we highlighted COG8 and Rab5C, two known and
202 well characterized positive regulators of PS-ASOs productive trafficking and activity in
203 different cell lines[35,36]. This finding further supports the validation and robustness of our
204 screening experiment. As a first set of genes, we selected Elmo Domain Containing 1
205 (ELMOD1), Fumarate Hydratase (FH), Transcriptional Adapter 2-Beta (TADA2B) and
206 Williams-Beuren Syndrome Chromosome Region 16 (WBSCR16), which are from to the top
207 ranked candidates with 4 sgRNAs fulfilling the chosen criteria. We also selected WDR91 as it
208 is an important factor that participates in the negative regulation of phosphatidylinositol–3–
209 phosphate (PtdIns3P) allowing the early-to-late endosome conversion[45,46]. This first pool of 5
210 genes was considered as a nonbiased sampling of potential activator candidates to be further
211 investigated.

212

213 **WDR91 promotes tcT3 ASO activity in 501Mel cells**

214 An RNA interference experiment was designed to further validate the five selected candidates
215 as ASO activity enhancers (Figure 5A). After protein knockdown, the tcT3 activity should be
216 reduced resulting in increased cell proliferation compared to a control condition.

217 It was already well established in previous *in vitro* studies that the protein ANXA2 was an
218 important facilitator of PS-ASOs endosomal trafficking in various cell lines[37]. We thus first
219 evaluated the effect of ANXA2 downregulation in 501Mel cells proliferation with or without
220 tcT3 in comparison with a control siRNA. A western blot analysis confirmed the
221 downregulation of ANXA2 protein after cells treatment with an ANXA2 siRNA
222 (Supplementary Figure 3A). As shown in Figure 5B, *ANXA2* mRNA knockdown significantly
223 impaired the activity of tcT3 by comparison with a control siRNA.

224 As for ANXA2, each individual candidate (WBSCR16, TADA2B, FH, ELMOD1 and WDR91)
225 was downregulated with a corresponding siRNA (or a control siRNA) for 48h. The knockdown
226 efficiencies were confirmed by qPCR analysis (Supplementary Figure 3B – Apart from
227 ELMOD1, all knockdowns were shown to be significant enough to allow a relevant biological
228 effect). 501Mel cells were then reverse transfected with either the siRNA alone or a
229 combination of siRNA and tcT3. Four days after the second transfection, the cell density was
230 measured by a crystal violet colorimetric assay (Figure 5A). After normalizing the cell density
231 in each condition to the non-treated one, WDR91 and WBSCR16 showed a significant
232 inhibition of tcT3 anti-proliferative activity (Figure 5C and Supplementary Table 2). To discard
233 any bias introduced by a siRNA treatment non-specific effect on the proliferation, the cell
234 density in each siRNA + tcT3 condition was then normalized to each of the corresponding
235 single siRNA treatment. In these conditions, WDR91 knockdown cells showed the most
236 significant and reproducible inhibition of tcT3 anti-proliferative activity (Figure 5D).
237 Melanoma cells proliferation can also be promoted by the level of *TYRP1* mRNA expression[38].
238 qPCR analysis show that *TYRP1* mRNA expression level is not significantly affected by the

239 transfection of control, ANXA2 or WDR91 siRNAs (Supplementary Figure 3C). Therefore, we
240 decided to focus on WDR91 in our next investigations.

241

242 **WDR91 enhancer activity is PS-ASO sequence dependent**

243 We identified WDR91 using a fully modified TSB ASO made of tcDNA and wondered whether
244 similar effects would hold true in a different system (different mechanism of action, chemistry
245 and cell line). Indeed, it is known that human cancer cell lines have very heterogenous ASO
246 uptake efficiencies. To address this question, we first transfected the U2OS osteosarcoma cell
247 line with siRNAs (control or directed against ANXA2 or WDR91) and evaluated the effect on
248 LNA GMs activity (mRNA knockdown) directed against Metastasis Associated Lung
249 Adenocarcinoma Transcript 1 (*MALAT1*) and Inhibitor of Growth Family Member 2 (*ING2*)
250 RNAs. From these two RNAs, *MALAT1* is a highly studied and conserved nuclear lncRNA and
251 is abundantly expressed in many cells. The experimental workflow is depicted in Figure 6A.
252 RT-qPCR in control-siRNA conditions confirmed the efficient downregulation of *MALAT1* and
253 *ING2* mRNAs by their respective GM (Figure 6B). No impact was observed regarding either
254 MALAT1 or ING2 ASO-mediated mRNAs knockdowns after ANXA2 downregulation.

255 We observed that WDR91 knockdown efficiently abrogated MALAT1 ASO activity (Figure
256 6C), confirming the putative role of this protein in ASO potency. However, no such effect was
257 observed on ING2 ASO activity. Both 16-mers MALAT1 and ING2 GMs have the same design
258 and chemistry and only differ by their respective sequence. Considering that proteins interact
259 with ASOs in a sequence dependent manner[47], this suggests that WDR91 activity is PS-ASO
260 sequence dependent.

261 Together, these data highlight for the first time, a set of proteins that can modulate PS-ASO
262 potency in a melanoma cell line, and in a physiological context. Among these candidates,

263 WDR91 is a strong regulator. Its activity has been confirmed in two distinct cell lines but could
264 be ASO-sequence dependent.

265

266 **WDR91 does not influence PS-ASOs activity in muscle cells**

267 To evaluate the potency of WDR91 to affect PS-ASOs activity in a different context, we
268 assessed WDR91 ability to influence the activity of a splice-switching ASO used to mediate
269 exon skipping in skeletal muscle cells. ASO-mediated exon-skipping is indeed one of the most
270 promising therapeutic approaches for the treatment of Duchenne muscular dystrophy (DMD).
271 The mechanism of action of ASO in this context is to mask important regulatory splicing signals
272 to exclude the targeted exon and restore the reading frame of the DMD pre-mRNA[48].
273 Immortalized human myoblasts from DMD patients are typically used as a model to study
274 dystrophin restoration mediated by splice switching oligonucleotides (SSOs). Here we used
275 immortalized DMD myoblasts carrying a deletion of DMD exon 52 leading to an out-of-frame
276 mRNA and resulting in the absence of dystrophin. The use of an SSO directed against the exon
277 51 (SSOEx51) allows to restore the open-reading frame of the dystrophin mRNA.

278 To study the effect of WDR91 on SSOEx51 activity, the immortalized KM571 cells were first
279 transfected with siRNAs to knockdown WDR91 or ANXA2 expression (Figure 7A). Seventy-
280 two hours later cells were treated with the SSOEx51 (LNA/2'OMe PS mixmer) to study exon
281 51 skipping efficiency in a context where WDR91 or ANXA2 expression was reduced. RNA
282 was extracted to first check knockdown efficiency, and we confirmed that siRNAs treatment
283 resulted in a strong knockdown (>70 %) of *WDR91* and *ANXA2* respective mRNAs (Figure
284 7B). Exon skipping levels were then compared and normalized to the siRNA control group
285 (siCTL). We noted a significant reduction in the exon skipping efficacy when ANXA2
286 expression was reduced (Figure 7C). However, this effect was not observed with WDR91.

287 Similar results were obtained with a different SSO chemistry (2MOE PS) (Supplementary
288 Figure 4), indicating that WDR91 is not a modulator of PS-ASOs in this system.

289 To determine whether this effect was specific to SSOs or to KM571 cells, we used a different
290 type of ASO to clarify the role of WDR91 in these cells. As described above, we first transfected
291 the KM571 cells with siRNAs targeting *WDR91* or *ANXA2* mRNAs and then with a GM against
292 *MALAT1* mRNA (GM MALAT1) (Figure 7D). Here again, siRNA-induced knockdown of
293 *WDR91* and *ANXA2* was very efficient (Figure 7E). When quantifying the levels of *MALAT1*
294 mRNA, we observed no significant differences between the siRNA treatment (control, ANXA2
295 or WDR91) (Figure 7F) indicating that WDR91 or ANXA2 knockdown did not affect GM
296 MALAT1 activity. These results suggest that WDR91 likely does not contribute to PS-ASO
297 activity in KM571 cells, regardless of the type of PS-ASOs used.

298

299 DISCUSSION

300 Despite many clinical successes, the precise mechanisms of ASOs uptake and trafficking
301 remain to be fully understood. In this study, we used a genome-wide CRISPR inhibition screen
302 to identify without *a priori* proteins involved in PS-ASO trafficking, release and productive
303 activity in a 501Mel cell line. Our CRISPR knockout screening strategy has enabled us to
304 discover functionally involved proteins, using a 3rd generation ASO and preserving the integrity
305 of intracellular membranes and organelles. Moreover, the miRNA displacement mediated by a
306 Target Site Blocker ASO represents a relevant assay to investigate the proteins involved in
307 ASOs efficiency and which has been validated *in vivo*.

308 This study revealed a set of 95 potential activators and 55 inhibitors. Among the activators, our
309 assay highlighted the Rab5C and COG8 proteins, which are known positive regulators of ASOs
310 trafficking and productive activity[35,36]. ANXA2, which is another known positive regulator,

311 was not found in the list of candidates after application of our filters, which also shows that this
312 type of CRISPR screen can be subject to false negatives.

313 In this study, we focused on WDR91 protein as a candidate of interest. This protein has a strong
314 biological relevance as it is known to participate in the early-to-late endosome conversion and
315 its knockdown showed the most significant inhibition of tcT3 anti-proliferative activity in our
316 validation experiments.

317 We confirmed that WDR91 was a positive modulator of PS-ASO activity in two different
318 assays (cell density assay and mRNA knockdown performance), with different cell models
319 (501Mel and U2OS) and ASO chemistries (tcDNA TSB and LNA GM), a landmark result of
320 this project. The impact of WDR91 was not validated in all the systems studied. Indeed,
321 although our results are similar when comparing the ASO activity of WDR91 in 501Mel and
322 U2OS cells, they tend towards an ASO sequence-related activity. In addition, WDR91 did not
323 have any effect with a splice-switching ASO in muscle cells. Thus, as is the case for ANXA2,
324 WDR91 may have an ASO-promoting activity that is also cell line-dependent. Indeed, it is
325 known that identified proteins involved in ASO trafficking and productive activity might not
326 have the same impact depending on the cell line (probably due to differences in high isoform
327 co-expression or the establishment of compensatory proteins or pathways). The same
328 observation was made, for example, in a study evaluating Rab5C, a well-characterized
329 modulator of ASO activity[49].

330 Ultimately, the results of our validation experiments on various cell systems and ASO
331 chemistries underline the need for caution when identifying an ASO modulator in a specific
332 context, as it may not be applicable to all systems.

333 Interestingly, other studies have highlighted WDR91 as an important mediator of the release
334 and efficacy of internalized reoviruses or antibody-drug conjugates in cells during the early

335 endosome maturation or from the late endosomes[50,32]. Therefore, this study tends to further
336 reinforce the key role of endosomal proteins in productive ASO trafficking and activity.

337 One of the limitations of our study is that genome-wide CRISPR screening was performed in a
338 single replicate. Rigorous filters were used to identify robust ASO activity modulators. We
339 have chosen to focus on a few selected proteins that promote internalized ASO activity, but it
340 would also be interesting to validate other identified proteins as well as the potential inhibitors
341 to confirm other candidates in 501Mel cells, as well as in other melanoma cell lines with
342 different states of cell differentiation. Furthermore, and given the specificity of this cell type
343 with regard to melanosome biogenesis and transport, involving numerous traffic processes[51], it
344 would be of interest to further evaluate WDR91 in other cell lines as it has been done in U2OS
345 and KM571 cells.

346 Analysis of the gene set enrichment also suggested new avenues to explore. Looking at the
347 inhibitory proteins, some of them were associated with the endosomal cellular compartment.
348 ATP6V0D2, for example, is one of the strongest inhibitor candidates in our selection and is
349 involved in the acidification and pH maintenance in certain intracellular compartments[52]. Some
350 activator candidates might be related to actin cytoskeleton regulation. From the related proteins,
351 CDC42 and MAP2 are known to be involved in cellular trafficking disorders[53]. It is therefore
352 relevant to consider that a defect in these proteins could also have an impact on intracellular
353 trafficking and ASO release in melanoma.

354 Ultimately, our results contribute to a better characterization and identification of protein
355 modulators of ASO activity, providing valuable information for potential new therapeutic
356 avenue. Potent ASO modulators validated *in vitro* could be inhibited or overexpressed in *in*
357 *vivo* experiments to assess and confirm an increase in ASO potency. Acting at the level of these
358 modulators or directly on ASO-modulators interaction could result in more productive ASO

359 activity, triggering an exacerbated inhibitory effect and an overall increase in the therapeutic
360 index.

361

362 MATERIALS AND METHODS

363 **Cell lines and lentiviral library**

364 501Mel and U2OS cells were acquired from ATCC. Before experiments, all cells were
365 regularly tested for absence of mycoplasma. Culture and sub-culturing were performed in
366 RPMI-1640 (Gibco) for 501Mel and Mc Coy's 5A (Gibco) for U2OS, supplemented with 10%
367 fetal bovine serum (FBS) (Gibco), 2mM L-glutamine (Gibco) and 1% penicillin/streptomycin,
368 (Gibco) and cultured at 37°C in a humidified incubator with 5% CO_2. Transfections and
369 infections were performed in the same media but without antibiotics and with a
370 decomplemented serum (30 minutes at 56°C). Immortalised myoblasts carrying a deletion of
371 DMD exon 52 (KM571) were obtained from the platform for immortalization of human cells
372 from the Institut de Myologie. KM571 cells were grown in a 50/50 mix of skeletal muscle cell
373 growth medium (Promocell, Germany) and F-10 (Thermo Fisher Scientific, USA) with 10%
374 fetal bovine serum, and 1% penicillin-streptomycin (100 U/mL).

375

376 **Antisense oligonucleotides**

377 miRCURY LNA™ Target site blockers TSB-C1 (ACTTTATTACAATCAT) and TSB-T3
378 (ACACAGTGGCAAACAC) were designed and obtained from Qiagen. tcC1 and tcT3 were
379 synthesized from SQY Therapeutics (Montigny le Bretonneux) as fully modified tcDNA-PS
380 ASOs. The TSB-C1 and tcC1 controls have no significant match to any annotated human
381 3'UTR. MALAT1 (CGTTAACTAGGCTTTA) and ING2 (TACGTTGGCTTGTTCA) LNA

382 Gapmers were designed and obtained from Qiagen. For the KM571 experiments, all ASOs were
383 obtained from Eurogentec. Two chemistries of the splice switching oligonucleotide targeting
384 exon 51 (SSOEx51 previously described in Saoudi et al., 2023[54]) were used: LNA/2'OMe PS
385 mixmer and full 2MOE PS. MALAT1 GM is a 2MOE PS (previously described in Wang et al.,
386 2016[37]). All ASOs were reconstituted in nuclease-free water (Invitrogen).

387

388 **siRNAs**

389 siRNAs pools were purchased from Santa Cruz (Negative Control A sc-37007; WDR91 sc-
390 89398; WBSCR16 sc-89899; FH sc-105377; ELMOD1 sc-77261; TADA2B sc-156169;
391 ANXA2 sc-270151)

392

393 **Generation of 501Mel knockout library**

394 Transduction of mycoplasma negative 501Mel cells at 60% confluence was performed in T175
395 flasks (standard - Sarstedt) with the Brunello knockout pooled lentiviral library from Addgene
396 (# 73179-LV) and in RPMI-1640 decomplemented medium (Gibco) without antibiotics. The
397 Brunello pooled lentiviral library contains 76,441 single guides RNAs (sgRNAs), targeting
398 19,114 coding genes (4 sgRNAs per gene). A multiplicity of infection (MOI) of 0.4 was
399 selected to ensure that every single cell is infected with only one sgRNA. Twenty-four hours
400 later, the infectious medium was replaced by a fresh complete medium. After 48h, infected cells
401 were positively selected with 2.5µg/mL puromycin (InvivoGen) for 7 days. Following selection
402 and expansion of the surviving cells, around 350 million cells were recovered. A dry pellet of
403 100 million cells was prepared for gDNA extraction and sequencing. The remaining cells were
404 used for the subsequent reverse transfection.

405

406 **RNA interference, ASO treatments and cell density assay**

407 **501Mel parental cells.** Reverse-transfections of siRNAs were performed in 60mm dishes
408 (standard - Sarstedt) with 224,000 cells per dish and for 48h in RPMI-1640 decomplemented
409 medium without antibiotics. Briefly, 1mL lipoplexes layers were formed with Lipofectamine
410 2000 (Invitrogen) and the siRNA concentrations were set to 30nM in a final 3mL volume after
411 addition of the cells on top of the lipoplexes. For all the transfections, lipoplexes were formed
412 in OptiMEM®. After 16h incubation, the medium was replaced by a fresh complete medium
413 without antibiotics. After 48h, the cells were recovered, counted with a Neubauer counting
414 chamber and a second reverse-transfection was performed in 96-well plates (standard F-
415 Sarstedt) with 3000 cells per well and with either the siRNA alone (at 30nM final concentration)
416 or a combination of siRNA (30nM) and tcT3 at a final concentration of 50nM in a final volume
417 of 150µL (100µL of cells on top of 50µL of lipoplexes). After 16h incubation, the medium was
418 replaced by a fresh 150µL complete medium without antibiotics. After 4 days following to the
419 second transfection, the cell density was measured with 0.5% crystal violet (10 minutes at RT,
420 followed by three PBS washes, 100µL of 100% EtOH solubilization and absorbance reading at
421 590nm using a Tecan Infinite F200 Pro reader).

422 **U2OS cells.** Reverse-transfections of siRNAs were performed in 12-well plates (standard -
423 Sarstedt) with 50,000 cells per well and for 48h in decomplemented Mc Coy's 5A medium
424 without antibiotics. Cell density was optimized so these cells are efficiently transfected between
425 20 and 30% confluence. The procedure was the same as described above except that the siRNA
426 transfection was performed with RNAiMax (Invitrogen) and 6h post seeding. After 48h, the
427 medium was replaced by 0.4mL of a fresh decomplemented Mc Coy's 5A medium without
428 antibiotics and a reverse-transfection with Lipofectamine 2000 was performed in the same plate

429 with the MALAT1 or ING2 Gapmer (at 30nM final concentration) in a final volume of 0.8mL
430 (0.4mL of lipoplexes on top of the cells). After 24h following to the second transfection, total
431 RNA was extracted for further RT-qPCR analysis.

432 **501Mel knockout library.** Reverse-transfections of tcT3 and C1 were performed in 150mm
433 dishes (standard - Sarstedt) with 1.5 million knockout cells per dish and for 72h in RPMI-1640
434 decomplemented medium without antibiotics. Briefly, 10mL lipoplexes layers were formed
435 with Lipofectamine 2000 (Invitrogen) and the respective ASOs concentrations were set to
436 50nM in a final 24mL volume after addition of the cells on top of the lipoplexes. For the
437 transfections, lipoplexes were formed in OptiMEM® and the mycoplasma-negative knockout
438 cells have been sub-cultured 24h before in T175 flasks (standard - Sarstedt). The cells
439 confluency at the day of transfection was maintained between 50 and 80%. After 7h of
440 transfection, the medium was replaced by a fresh complete medium without antibiotics. To
441 ensure a coverage of 400 cells per guide RNA in our library, a total of 32 million cells was
442 transfected with either the tcT3 or C1. Thus, 22 dishes were used per oligonucleotide
443 transfection. After 72h of transfection, surviving cells were recovered and pellets of 100 million
444 cells were kept at -80°C until further processing.

445 **KM571 cells.** Cells were plated in 6-well plates (300,000 cells per well) and transfected the
446 same day with 20nM of siRNA with Lipofectamine RNAiMAX according to the
447 manufacturer's instructions (Thermo Fisher Scientific, USA). Twenty-four hours after the first
448 transfection, proliferation medium was changed for differentiation medium (DMEM, 2% horse
449 serum, 1% penicillin / streptomycin (100 U/mL)) to induce myotubes formation. After 3 days
450 of differentiation, cells were treated with 100nM of the SSOEx51 for 24h with Lipofectamine
451 LTX according to the manufacturer's instructions (Thermo Fisher Scientific, USA). For the
452 transfection of the GM MALAT1, similar protocol was used, except that KM571 cells were
453 only treated during proliferation and that the GM MALAT1 treatment was performed for 48h.

454

455 **NGS sequencing library preparation**

456 Frozen pellets of 100 million transfected surviving cells (and from non-treated knockout
457 library) in 50mL poplypropylene tubes (Sarstedt) were thawed on ice for 20 minutes and lysed
458 at room temperature. Genomic DNA was purified according to the manufacturer's instructions
459 (NucleoBond HMW DNA, Macherey-Nagel). A total of 280µg of genomic DNAs was used for
460 PCR amplification of sgRNA sequences, using the Herculase II Fusion polymerase (Agilent).
461 Illumina P5- and P7-barcoded adaptors were used, and PCR amplification and quality controls
462 have been carried out as described by Zhang laboratory (Joung *et al*, 2017). Amplified PCR
463 products were purified using AMPure XP beads (Beckman Coulter) according to the
464 manufacturer's instructions, eluted in 14µL of nuclease-free water (Invitrogen) and stored at -
465 20°C until Bioanalyzer quality control (TapeStation 4200, Agilent) was used to measure the
466 size, quality and concentration. The pooled samples were sequenced using Illumina NGS
467 sequencing platform (Novaseq6000 – CurieCoreTech ICGex Platform).

468

469 **NGS data analysis**

470 MAGeCK (v0.5.9.4) was used to extract sgRNA read counts from the samples fastq.gz files
471 (mageck count program with the --norm-method median option). For each sgRNA, we
472 transformed the read counts onto M (log ratio) and A (mean average): M =
473 log2(sgRNA_count_in_TRT+1) - log2(sgRNA_count_in_CTL+1), and A = mean
474 (count_TRT, count_CTL) in log2 scale. Fold-changes between TRT and CTL conditions were
475 also computed from the M values of each sgRNA.

476

477 **RNA extraction and RT-qPCR analysis**

478 Total RNA form cell lysates was obtained using a NucleoSpin® RNA kit (Macherey-Nagel),
479 according to the manufacturer's instructions and with on-column DNAse treatment. After
480 Nanodrop evaluation of purity and concentration, 500ng of RNA was used for reverse-
481 transcription (MultiScribe RT – Applied Biosystems). Obtained cDNA was diluted to 2.5ng/µL
482 and used as template for qPCR using a QuantStudio5 system (Applied Biosystems). SYBR
483 Green (PowerSYBR® Green PCR Master Mix – Applied Biosystems) was used according to
484 the manufacturer's instructions. For each sample measurement, 3 technical replicates were
485 performed. TBP was used as internal standard. TYRP1 and ING2 primers were purchased from
486 Eurogentec. % knockdown was calculated as $100*(1-2^{-ddCt})$. Total RNA was isolated from
487 cultured human myoblast cells using TRIzol reagent, according to the manufacturer's
488 instructions (Thermo Fisher Scientific, USA). Aliquots of 1 µg of total RNA were used for RT-
489 PCR analysis. The cDNA synthesis was carried out with LunaScript™ RT SuperMix Kit (New
490 England Biolabs). Exon 51 skipping was measured by TaqMan qRT-PCR, using TaqMan
491 assays that were designed against the exon 51-53 or exon 50-53 templates using the Prime Time
492 qPCR probe assays (Integrated DNA Technology) (Assay Ex51-53 - forward : 5'-
493 CAGGTTGTGTCACCAGAGTAA-3'; reverse 5'-TGAGTGGAAGGCGGTAAA-3'; probe :
494 5'-/56-FAM/TGACCACTA/ZEN/TTGGAGCCTCTCCTAC/3IABkFQ/-3' and assay Ex50-
495 53: forward: 5'-ACTGATTCTGAATTCTTTCAAAGGC-3'; reverse: 5'-
496 TTCAAGAGCTGAGGGCAAAG-3'; probe: 5'- /56-
497 FAM/ACCTAGCTC/ZEN/CTGGACTGACCACT/3IABkFQ/-3') . gBlocks Gene Fragments
498 (Integrated DNA Technology) from human exon 49-54 and human exon 49-54 Delta 52 were
499 used as standards for DNA copy number. 70 ng of cDNA was used as input per reaction, and
500 all assays were carried out in triplicate. Assays were performed under fast cycling conditions
501 on a Bio-Rad CFX384 Touch Real-Time PCR Detection System. For a given sample, the copy

502 number of skipped product (exon 50-53 assay) and unskipped product (exon 51-53 assay) was
503 determined using the standards Ex49-54 and Ex49-54 Delta52, respectively. Exon 51 skipping
504 was then expressed as a percentage of total dystrophin. Knockdown analysis was performed by
505 using the appropriate probes for the studied targets and were purchased from Integrated DNA
506 technologies (IDT) (MALAT1 Hs.PT.58.26451167.g; WDR91 Hs.PT.58.39523053 and
507 ANXA2 Hs.PT.56a.40676274). The expression of the different targets was then normalized to
508 a reference gene (GAPDH Hs.PT.39a.22214836).

509

510 **Protein isolation and Western blotting**

511 Total protein extracts were obtained by resuspension of PBS-washed cell pellets in 40µL of
512 ice-cold RIPA buffer (Tris-HCl 50 mM, ph7.4, NaCl 150 mM, Sodium Deoxycholate 0.5%,
513 Triton 1%, SDS 0.1%), including protease inhibitor cocktail (Sigma-Aldrich, P8340) and
514 centrifugation at 16,000xg for 15min at 4°C. Proteins quantification from the cleared lysates
515 was performed using a Pierce™ BCA Assay kit (Thermo scientific). After 4-12% SDS-PAGE
516 in NuPAGE MES buffer (Invitrogen), proteins were transferred onto PVDF membranes with a
517 turbo transfer system (BIO-RAD) for 10 minutes at 25V and 2.5A. After transfer, the
518 membranes were washed in Tris-buffered saline and 0.1% Tween 20 (TBST) and blocked for
519 30 minutes at room temperature in a solution of TBST + 5% w/v non-fat dry milk. Blocked
520 membranes were washed three times in TBST for 5 minutes and diluted primary antibody was
521 incubated at 4°C overnight with shaking. The diluted HRP-conjugated secondary antibody was
522 added for 1h at room temperature with shaking, after three TBST washes of 5 minutes. Imaging
523 was performed after ECL reagent addition and chemiluminescence detection with G:Box
524 Chemi XX6 imager from Syngene. ANXA2 antibody was purchased from Santa Cruz (sc-
525 28385).

526

527 **Statistical analysis**

528 GraphPad Prism software (San Diego, CA, USA) version 9.5.1 was used for statistical analysis
529 and graphs design. Each data is presented as mean of at least three independent biological
530 replicates with standard deviation (SD). P-values were calculated by two-sided unpaired *t*-tests
531 with Welch's correction and differences were statistically significant at $*p \leq 0.05$; $**p \leq 0.01$;
532 $***p \leq 0.001$; $****p \leq 0.0001$. For exon skipping experiments, normal distribution of samples
533 was assessed by using Shapiro-Wilk test. Comparisons of statistical significance were assessed
534 by one-way ANOVA parametric test or Kruskal-Wallis non-parametric test and followed by
535 appropriate post-hoc tests if applicable.

536

537 DATA AVAILABILITY STATEMENT

538 Data are available upon request to the corresponding author.

539

540 KEYWORDS

541 CRISPR screen; NGS; Antisense Oligonucleotides (ASOs); Melanoma; Target Site Blockers;
542 protein modulators of ASOs; endosomes; productive activity; WDR91.

543

544 ACKNOWLEDGMENTS

545 The authors thank the SFR Biosit L3 platform of Rennes University for providing the required
546 facility for performing the lentiviral infections. The authors also thank the Institut Curie
547 (Genetic screen CRISPR'it and ICGex Core Facilities) for performing the NGS sequencing,

548 SQY Therapeutics for providing the tcDNA-ASO molecules and the platform for the
549 immortalization of human cells from the Institut de Myologie for the human-derived cells. This
550 study received financial support from the Agence Nationale de la Recherche (ANR).

551

552 AUTHOR CONTRIBUTIONS

553 G.M., R.P., A.Go. and A.Ga. conceived and analyzed the experiments. G.M. and A.Ga.
554 performed the experiments. M.A. analyzed the NGS raw data. A.M. and A.B. helped in the
555 library preparation. G.M. wrote the manuscript. All the authors reviewed the manuscript.

556

557 DISCLOSURE AND COMPETING INTERESTS STATEMENT

558 The authors declare no competing financial interests.

559

560 FIGURE LEGENDS

561 **Figure 1. Inhibition of 501Mel cells proliferation with Target Site Blocker ASOs targeting**
562 ***TYRP1* mRNA.** (A) A competition mechanism occurs with binding of TSB-T3 to a sequence
563 overlapping the miR-16 site in the 3'UTR of *TYRP1* mRNA, thus releasing miR-16 whose
564 tumor suppressor activity is restored. TSB-C1 (Control ASO) has no match with *TYRP1*
565 3'UTR[38]. The cell density assay upon TSB-C1 or -T3 treatment is measured through a crystal
566 violet colorimetric assay. The figure 1A was generated with BioRender.com (B) 501Mel cell
567 density assay at day 3 with increasing concentrations of reverse-transfected LNA- (T3) or
568 tcDNA- (tcT3). Experiments were performed in independent biological triplicates. Data were
569 normalized to the corresponding control conditions (C1 or tcC1) at the same concentrations
570 (10, 30, 50 and 70nM). Data are presented as mean (SD). Unpaired *t*-test with Welch's

571 correction were performed. The statistical significance is **P=0,0040 (T3 *vs* C1 – 30nM);
572 *P=0,0241 (T3 *vs* C1 – 50nM); **P=0,0061 (T3 *vs* C1 – 70nM); **P=0,0078 (tcT3 *vs* tcC1 –
573 30nM); **P=0,0036 (tcT3 *vs* tcC1 – 50nM); *P=0,0105 (tcT3 *vs* tcC1 – 70nM).

574

575 **Figure 2. Generation and treatment of the 501Mel cells knockout library.** (A) Workflow
576 of the experimental setup. S1: Step 1 (cells transduction – non infected cells in grey on the
577 workflow); S2: Step 2 (transduced cells positive selection with antibiotic); S3: Step 3 (ASO
578 exposure); S4: Step 4 (gDNA purification and sgRNAs amplification). The figure was
579 generated with BioRender.com (B) Distribution of the number of normalized read counts per
580 sgRNA in the tcT3 and the tcC1-treated library. The mean is represented by a red bar (C)
581 Method for identifying genes promoting or inhibiting ASO uptake and/or efficiency after NGS
582 sequencing and based on normalized read counts after tcC1 or tcT3 treatment.

583

584 **Figure 3. NGS sequencing data sorting and analysis.** (A) After sgRNA extraction, MA plots
585 are used to visualize the differences between measurements (read counts) between two
586 conditions: treatment (tcT3) *versus* control (tcC1). For each sgRNA, the read counts are
587 transformed onto M (log ratio) and A (mean average) scales. M is equal to
588 log2(sgRNA_count_in_TRT+1) - log2(sgRNA_count_in_CTL+1) and A is the mean between
589 count_TRT and count_CTL in log2 scale. Candidates' selection was performed according to
590 the following criteria: $A \geq 6$ and $M \geq 0.6$ (enriched sgRNAs, ASOs activators); $A \geq 6$ and $M \leq$
591 -0.6 (depleted sgRNAs, ASOs inhibitors). Control sgRNAs (non-targeting guides) are located
592 between $M \geq 0.6$ and $M \leq -0.6$. On the obtained MA plot, red, green and black dots represent
593 the genes with the 4, 3 and 2 sgRNAs over 4 fulfilling the defined criteria, respectively (B) MA
594 plot examples from selected activator and inhibitor candidates with applied M and A filters and

595 with 4 (GGTLC2) or 2 relevant sgRNAs (WDR91). The yellow dots represent the genes with
596 a very low expression in either the treatment or the control condition and as a consequence, an
597 elevated but non-significant fold change (C) Representation of the post-sequencing normalized
598 read counts in the control (CTL – tcC1) and treated (TRT – tcT3) conditions for the sgRNAs
599 of four sorted modulator candidates (COG8, WBSCR16, WDR91, in red – activators; GGTLC2
600 in blue – inhibitor). The fold change is calculated as: tcT3 read counts / tcC1 read counts (for
601 activators); tcC1 read counts / tcT3 read counts (for inhibitors).

602

603 **Figure 4. ASO activators and inhibitors ranking and selection.** (A) Distribution of the
604 average fold change (tcT3 read counts *vs* tcC1 read counts) from the fold changes of the 2, 3 or
605 4 corresponding sgRNAs per gene, for 53 of the 95 selected ASO activator candidates (fulfilling
606 the criteria A ≥ 6 and M ≥ 0.6 on the MA plot). Green stars represent candidates that have
607 already characterized in the literature. Black stars correspond to the 5 candidates that have been
608 chosen for further functional validation (B) Distribution of the average fold change (tcC1 read
609 counts *vs* tcT3 read counts) from the fold changes of the 2, 3 or 4 corresponding sgRNAs per
610 gene, for 31 of the 55 selected ASO inhibitor candidates (fulfilling the criteria A ≥ 6 and M ≤ -
611 0.6 on the MA plot). The fold change threshold was fixed to 1.5. The full list activator and
612 inhibitor candidates is provided in Supplementary Table 1.

613

614 **Figure 5. Functional validation of tcT3 activity enhancer candidates in 501Mel cells.** (A)
615 Workflow of the experimental design (B) Setup of the 501Mel cell density assay with ANXA2
616 positive control. Cell density measurement was performed by crystal violet assay after tcT3
617 transfection on normal, control or ANXA2 knockdown cells (NT: Non-Treated; siCTL: control
618 siRNA). The relative cell density in each condition is normalized to the non-treated cells. (C)

619 501Mel cell density assay after tcT3 transfection on normal, control or candidate's knockdown
620 cells. Data are represented with a cell density normalized to the non-treated cells (100%) (D)
621 Same data as above but represented with a cell density normalized to 100% for each treatment
622 with the siRNA alone, to discard any proliferation bias induced by the siRNA's effects.
623 Experiments were performed in independent biological replicates. Data are presented as mean
624 (SD). Unpaired *t*-test with Welch's correction were performed. In the lower panel, the statistical
625 significance is *P=0,0468 (TADA2B, N=3); **P=0,0011 (WDR91, N=4); ****P≤0,0001
626 (ANXA2, N=5); NS= non-significant (P=0,0588).

627

628 **Figure 6. Functional validation of WDR91 in U2OS cells.** (A) Workflow of the experimental
629 design (B) *MALAT1* and *ING2* mRNA quantification by RT-qPCR at D4 and D5 respectively,
630 after corresponding GM transfection on non-treated, control or ANXA2 knockdown cells. The
631 relative mRNA fold change was normalized to the non-treated condition (no siRNA
632 transfection). Experiments were performed in independent biological triplicates (MALAT1)
633 and quadruplicates (ING2). Data are presented as mean (SD). Unpaired *t*-test with Welch's
634 correction were performed. The statistical significance is **P=0,0019 (NT *vs* siCTL);
635 ****P<0,0001 (NT *vs* siCTL; NT *vs* siANXA2) (C) *MALAT1* and *ING2* mRNA quantification
636 by RT-qPCR at D4 and D5 respectively, after corresponding GM transfection on non-treated,
637 control or WDR91 knockdown cells. The relative mRNA fold change was normalized to the
638 non-treated condition (no siRNA transfection). Experiments were performed in independent
639 biological triplicates (MALAT1) and quadruplicates (ING2). Data are presented as mean (SD).
640 Unpaired *t*-test with Welch's correction were performed. The statistical significance is
641 **P=0,0019 (NT *vs* siCTL); NS= non-significant (P=0,1755); ***P=0,0001 (NT *vs* siWDR91);
642 ****P<0,0001 (NT *vs* siCTL).

643

644 **Figure 7. Functional validation of WDR91 in an immortalized DMD muscle cell line**
645 **(KM571).** (A) Experimental setup for the double transfection protocol of siRNAs and SSOs in
646 KM571 (B) *WDR91* and *ANXA2* mRNAs silencing efficiency (siCTL: Control siRNA) (C)
647 *WDR91* and *ANXA2* mRNAs silencing effects on exon 51 skipping efficiency of the SSOEx51
648 (D) Experimental setup for the double transfection protocol of siRNAs and a GM against
649 MALAT1 (GM MALAT1) in KM571 (E) *WDR91* and *ANXA2* mRNAs silencing efficiency
650 (siCTL: Control siRNA) (F) *WDR91* and *ANXA2* mRNAs silencing effects on MALAT1
651 knockdown induced by the GM MALAT1. Results are shown as the average of at least four
652 independent biological replicates. Data are presented as mean (SD). The relative mRNA fold
653 change was normalized to the appropriate control condition (Mock or siCTL). Unpaired *t*-test
654 with Welch's correction were performed. The statistical significance is ** P <0,005;
655 ****P<0,00005.

656

657 **Supplementary Figure 1. Gene set enrichment analysis on activator candidates.** Gene set
658 enrichment analysis using PANGEA (Pathway, Network and Gene-set Enrichment Analysis)
659 allowed to classify the activator candidates based on the cellular component gene ontology.
660 Each gene set is classified according to its highest value (log2 fold change). In green are framed
661 the proteins that are part of the peroxisome cellular component. In red are framed the proteins
662 that are part of the mitochondrion cellular component. In purple are framed the proteins that are
663 part of the actin cytoskeleton cellular component. The color code and corresponding lines
664 highlight common candidates between each corresponding cellular component.

665

666 **Supplementary Figure 2. Gene set enrichment analysis on inhibitor candidates.** Gene set
667 enrichment analysis using PANGEA (Pathway, Network and Gene-set Enrichment Analysis)
668 allowed to classify the inhibitor candidates based on the cellular component gene ontology.
669 Each gene set is classified according to its highest value (log2 fold change). In green are framed
670 the proteins that are part of the Golgi apparatus cellular component. In red are framed the
671 proteins that are part of the microtubule cytoskeleton cellular component. In purple are framed
672 the proteins that are part of the endosomal cellular component. The color code and
673 corresponding lines highlight common candidates between each corresponding cellular
674 component.

675

676 **Supplementary Figure 3.** (A) Western blot analysis of ANXA2 protein expression at 48h and
677 72h on non-treated 501Mel cells and after ANXA2 or control siRNA reverse transfections. NT:
678 non-treated; siANXA2: ANXA2 siRNA; siCTL: Negative control siRNA. Alpha-tubulin was
679 used as a loading control (B) Evaluation and quantification of the candidate's knockdown
680 efficiency by RT-qPCR on total RNAs coming from non-treated (NT) or siRNA transfected
681 501Mel cells. Data are calculated from three technical replicates. % knockdown (KD) was
682 calculated as $100*(1-2^{-ddCt})$. TBP was used as housekeeping gene (C) TYRP1 mRNA
683 quantification by RT-qPCR on total RNAs coming from non-treated (NT) or siRNA transfected
684 501Mel cells (CTL: control siRNA). Results are shown as the mean of at least three independent
685 biological replicates (SD).

686

687 **Supplementary Figure 4. WDR91 do not affect the activity of a methoxyethyl chemistry**
688 **splice switching oligonucleotide in DMD muscle cells.** SSOEx51 used in these experiments
689 is an 2MOE PS. (A) *WDR91* and *ANXA2* mRNAs silencing efficiency (siCTL: Control siRNA)

690 (B) *WDR91* and *ANXA2* mRNAs silencing effects on exon 51 skipping efficacy of the SSOEx51
691 2MOE PS. Results are shown as the average of at least four independent biological replicates.
692 Data are presented as mean (SD). The relative mRNA fold change was normalized to the
693 appropriate control condition (Mock or siCTL). P-value was calculated by two-sided unpaired
694 t-tests against the Mock transfected or control siRNA condition. The statistical significance is
695 ** P <0.005; ****P<0.00005.

696

697 **Supplementary Table 1. Detailed list of the ASO activator and inhibitor candidates sorted**
698 **after applying M, A and fold change filters.** The corresponding 95 and 55 activator and
699 inhibitor candidates are represented with their respective sgRNAs fulfilling the defined criteria.
700 M (log ratio) = log2(sgRNA_count_in_TRT+1) - log2(sgRNA_count_in_CTL+1); A (Mean
701 average) = mean (count_TRT, count_CTL) in log2 scale. Fold-changes (FC) between TRT
702 (tcT3-treated cells) and CTL (tcC1-treated cells) conditions were computed from the M values
703 of each sgRNA as FC (activator) = TRT read counts / CTL read counts; FC (inhibitor) = CTL
704 read counts / TRT read counts. KO is the number of read counts in the parental non-treated
705 knockout library. d value represents the absolute difference between the CTL and the TRT read
706 counts.

707

708 **Supplementary Table 2. Quantification by absorbance at 590nm of the cell density after**
709 **crystal violet coloration.** Raw absorbance data after candidate's knockdown and measure of
710 the inhibition of tcT3 anti-proliferative activity after four days of ASO treatment. Cell density
711 was measured with 0.5% crystal violet (10 minutes at RT, followed by three PBS washes,
712 100uL of 100% EtOH solubilization and absorbance reading at 590nm using a Tecan Infinite
713 F200 Pro reader). N1 to N8 are the biological replicates.

714

715 REFERENCES

[1] Stanley T. Crooke et al., "Antisense Technology: A Review," *The Journal of Biological Chemistry* 296 (February 16, 2021): 100416, https://doi.org/10.1016/j.jbc.2021.100416.

[2] J. Kim et al., "Patient-Customized Oligonucleotide Therapy for a Rare Genetic Disease," *The New England Journal of Medicine* 381, no. 17 (October 24, 2019): 1644–52, https://doi.org/10.1056/NEJMoa1813279.

[3] Stanley T Crooke et al., "Cellular Uptake and Trafficking of Antisense Oligonucleotides," *Nature Biotechnology* 35, no. 3 (March 1, 2017): 230–37, https://doi.org/10.1038/nbt.3779.

[4] Xin Xie et al., "Recent Advances in Targeting the 'Undruggable' Proteins: From Drug Discovery to Clinical Trials," *Signal Transduction and Targeted Therapy* 8, no. 1 (September 6, 2023): 1–71, https://doi.org/10.1038/s41392-023-01589-z.

[5] Martin Egli and Muthiah Manoharan, "Chemistry, Structure and Function of Approved Oligonucleotide Therapeutics," *Nucleic Acids Research* 51, no. 6 (March 7, 2023): 2529–73, https://doi.org/10.1093/nar/gkad067.

[6] Tina Nie, "Eplontersen: First Approval," *Drugs*, February 28, 2024, https://doi.org/10.1007/s40265-024-02008-5.

[7] Haoyu Xiong, Rakesh N. Veedu, and Sarah D. Diermeier, "Recent Advances in Oligonucleotide Therapeutics in Oncology," *International Journal of Molecular Sciences* 22, no. 7 (March 24, 2021): 3295, https://doi.org/10.3390/ijms22073295.

[8] Maria Gagliardi and Ana Tari Ashizawa, "The Challenges and Strategies of Antisense Oligonucleotide Drug Delivery," *Biomedicines* 9, no. 4 (April 16, 2021): 433, https://doi.org/10.3390/biomedicines9040433.

[9] Suzan M Hammond et al., "Delivery of Oligonucleotide-based Therapeutics: Challenges and Opportunities," *EMBO Molecular Medicine* 13, no. 4 (April 9, 2021): e13243, https://doi.org/10.15252/emmm.202013243.

[10] R.L. Juliano et al., "Cellular Uptake and Intracellular Trafficking of Oligonucleotides: Implications for Oligonucleotide Pharmacology," *Nucleic Acid Therapeutics* 24, no. 2 (April 1, 2014): 101–13, https://doi.org/10.1089/nat.2013.0463.

[11] Alexander Klipp, Michael Burger, and Jean-Christophe Leroux, "Get out or Die Trying: Peptide- and Protein-Based Endosomal Escape of RNA Therapeutics," *Advanced Drug Delivery Reviews* 200 (September 1, 2023): 115047, https://doi.org/10.1016/j.addr.2023.115047.

[12] Steven F. Dowdy et al., "Delivery of RNA Therapeutics: The Great Endosomal Escape!," *Nucleic Acid Therapeutics* 32, no. 5 (October 1, 2022): 361–68, https://doi.org/10.1089/nat.2022.0004.

[13] Philippine Aupy et al., "The Use of Tricyclo-DNA Oligomers for the Treatment of Genetic Disorders," *Biomedicines* 6, no. 1 (December 22, 2017): 2, https://doi.org/10.3390/biomedicines6010002.

[14] "Delivery Is Key: Lessons Learnt from Developing Splice-switching Antisense Therapies | EMBO Molecular Medicine," accessed March 27, 2024, https://www.embopress.org/doi/full/10.15252/emmm.201607199.

[15] Feryal Alhamadani et al., "Adverse Drug Reactions and Toxicity of the Food and Drug Administration-Approved Antisense Oligonucleotide Drugs," *Drug Metabolism and Disposition: The Biological Fate of Chemicals* 50, no. 6 (June 2022): 879–87, https://doi.org/10.1124/dmd.121.000418.

[16] Xue-hai Liang et al., "Identification and Characterization of Intracellular Proteins That Bind Oligonucleotides with Phosphorothioate Linkages," *Nucleic Acids Research* 43, no. 5 (March 11, 2015): 2927–45, https://doi.org/10.1093/nar/gkv143.

[17] Stanley T. Crooke et al., "The Interaction of Phosphorothioate-Containing RNA Targeted Drugs with Proteins Is a Critical Determinant of the Therapeutic Effects of These Agents," *Journal of the American Chemical Society* 142, no. 35 (September 2, 2020): 14754–71, https://doi.org/10.1021/jacs.0c04928.

[18] Xue-Hai Liang et al., "Hsp90 Protein Interacts with Phosphorothioate Oligonucleotides Containing Hydrophobic 2′-Modifications and Enhances Antisense Activity," *Nucleic Acids Research* 44, no. 8 (May 5, 2016): 3892–3907, https://doi.org/10.1093/nar/gkw144.

[19] Colton M. Miller et al., "Stabilin-1 and Stabilin-2 Are Specific Receptors for the Cellular Internalization of Phosphorothioate-Modified Antisense Oligonucleotides (ASOs) in the Liver," *Nucleic Acids Research* 44, no. 6 (April 7, 2016): 2782–94, https://doi.org/10.1093/nar/gkw112.

[20] Thijs Van de Vyver, Stefaan C. De Smedt, and Koen Raemdonck, "Modulating Intracellular Pathways to Improve Non-Viral Delivery of RNA Therapeutics," *Advanced Drug Delivery Reviews* 181 (February 1, 2022): 114041, https://doi.org/10.1016/j.addr.2021.114041.

[21] Brendan T Finicle et al., "Simultaneous Inhibition of Endocytic Recycling and Lysosomal Fusion Sensitizes Cells and Tissues to Oligonucleotide Therapeutics," *Nucleic Acids Research* 51, no. 4 (February 28, 2023): 1583–99, https://doi.org/10.1093/nar/gkad023.

[22] Alexander N. Kapustin et al., "Antisense Oligonucleotide Activity in Tumour Cells Is Influenced by Intracellular LBPA Distribution and Extracellular Vesicle Recycling," *Communications Biology* 4 (November 1, 2021): 1241, https://doi.org/10.1038/s42003-021-02772-0.

[23] Timothy R. Wagenaar et al., "Identification of the Endosomal Sorting Complex Required for Transport-I (ESCRT-I) as an Important Modulator of Anti-miR Uptake by Cancer Cells," *Nucleic Acids Research* 43, no. 2 (January 30, 2015): 1204–15, https://doi.org/10.1093/nar/gku1367.

[24] Shiyu Wang et al., "Membrane Destabilization Induced by Lipid Species Increases Activity of Phosphorothioate-Antisense Oligonucleotides," *Molecular Therapy - Nucleic Acids* 13 (December 2018): 686–98, https://doi.org/10.1016/j.omtn.2018.10.011.

[25] Peter Lorenz et al., "Nucleocytoplasmic Shuttling: A Novel in Vivo Property of Antisense Phosphorothioate Oligodeoxynucleotides," *Nucleic Acids Research* 28, no. 2 (January 15, 2000): 582–92.

[26] "A Stress-Induced Response Complex (SIRC) Shuttles miRNAs, siRNAs, and Oligonucleotides to the Nucleus," accessed March 27, 2024, https://www.pnas.org/doi/epdf/10.1073/pnas.1721346115.

[27] Crooke et al., "The Interaction of Phosphorothioate-Containing RNA Targeted Drugs with Proteins Is a Critical Determinant of the Therapeutic Effects of These Agents."

[28] Liang et al., "Identification and Characterization of Intracellular Proteins That Bind Oligonucleotides with Phosphorothioate Linkages."

[29] Alfred Hanswillemenke et al., "Profiling the Interactome of Oligonucleotide Drugs by Proximity Biotinylation," *Nature Chemical Biology*, January 17, 2024, https://doi.org/10.1038/s41589-023-01530-z.

[30] Christoph Bock et al., "High-Content CRISPR Screening," *Nature Reviews Methods Primers* 2, no. 1 (February 10, 2022): 1–23, https://doi.org/10.1038/s43586-021-00093-4.

[31] Olivier Petitjean et al., "Genome-Wide CRISPR-Cas9 Screen Reveals the Importance of the Heparan Sulfate Pathway and the Conserved Oligomeric Golgi Complex for Synthetic Double-Stranded RNA Uptake and Sindbis Virus Infection," *mSphere* 5, no. 6 (November 11, 2020): e00914-20, https://doi.org/10.1128/mSphere.00914-20.

[32] C. Kimberly Tsui et al., "CRISPR-Cas9 Screens Identify Regulators of Antibody–Drug Conjugate Toxicity," *Nature Chemical Biology* 15, no. 10 (October 2019): 949–58, https://doi.org/10.1038/s41589-019-0342-2.

[33] Douglas Ross-Thriepland et al., "Arrayed CRISPR Screening Identifies Novel Targets That Enhance the Productive Delivery of mRNA by MC3-Based Lipid Nanoparticles," *SLAS Discovery* 25, no. 6 (July 2020): 605–17, https://doi.org/10.1177/2472555220925770.

[34] Moira A. McMahon et al., "GOLGA8 Increases Bulk Antisense Oligonucleotide Uptake and Activity in Mammalian Cells," *Molecular Therapy. Nucleic Acids* 32 (March 27, 2023): 289–301, https://doi.org/10.1016/j.omtn.2023.03.017.

[35] Colton M. Miller et al., "Endosomal Escape of Antisense Oligonucleotides Internalized by Stabilin Receptors Is Regulated by Rab5C and EEA1 During Endosomal Maturation," *Nucleic Acid Therapeutics* 28, no. 2 (April 1, 2018): 86–96, https://doi.org/10.1089/nat.2017.0694.

[36] Petitjean et al., "Genome-Wide CRISPR-Cas9 Screen Reveals the Importance of the Heparan Sulfate Pathway and the Conserved Oligomeric Golgi Complex for Synthetic Double-Stranded RNA Uptake and Sindbis Virus Infection."

[37] Shiyu Wang et al., "Annexin A2 Facilitates Endocytic Trafficking of Antisense Oligonucleotides," *Nucleic Acids Research* 44, no. 15 (September 6, 2016): 7314–30, https://doi.org/10.1093/nar/gkw595.

[38] David Gilot et al., "A Non-Coding Function of TYRP1 mRNA Promotes Melanoma Growth," *Nature Cell Biology* 19, no. 11 (November 2017): 1348–57, https://doi.org/10.1038/ncb3623.

[39] Arthur Gautron et al., "Human TYRP1: Two Functions for a Single Gene?," *Pigment Cell & Melanoma Research* 34, no. 5 (2021): 836–52, https://doi.org/10.1111/pcmr.12951.

[40] Philippine Aupy et al., "Identifying and Avoiding tcDNA-ASO Sequence-Specific Toxicity for the Development of DMD Exon 51 Skipping Therapy," *Molecular Therapy. Nucleic Acids* 19 (November 27, 2019): 371–83, https://doi.org/10.1016/j.omtn.2019.11.020.

[41] "Lowering Mutant Huntingtin Using Tricyclo-DNA Antisense Oligonucleotides As a Therapeutic Approach for Huntington's Disease - PubMed," accessed March 27, 2024, https://pubmed.ncbi.nlm.nih.gov/31184975/.

[42] John G Doench, "Am I Ready for CRISPR? A User's Guide to Genetic Screens," *Nature Reviews Genetics* 19, no. 2 (February 1, 2018): 67–80, https://doi.org/10.1038/nrg.2017.97.

[43] Kendall R. Sanson et al., "Optimized Libraries for CRISPR-Cas9 Genetic Screens with Multiple Modalities," *Nature Communications* 9 (December 21, 2018): 5416, https://doi.org/10.1038/s41467-018-07901-8.

[44] Yanhui Hu et al., "PANGEA: A New Gene Set Enrichment Tool for Drosophila and Common Research Organisms," *bioRxiv*, April 17, 2023, 2023.02.20.529262, https://doi.org/10.1101/2023.02.20.529262.

[45] Kai Liu et al., "WDR91 Is a Rab7 Effector Required for Neuronal Development," *Journal of Cell Biology* 216, no. 10 (October 2, 2017): 3307–21, https://doi.org/10.1083/jcb.201705151.

[46] Nan Liu, Kai Liu, and Chonglin Yang, "WDR91 Specifies the Endosomal Retrieval Subdomain for Retromer-Dependent Recycling," *The Journal of Cell Biology* 221, no. 12 (December 12, 2022), https://doi.org/10.1083/jcb.202203013.

[47] Timothy A. Vickers and Stanley T. Crooke, "Development of a Quantitative BRET Affinity Assay for Nucleic Acid-Protein Interactions," *PloS One* 11, no. 8 (2016): e0161930, https://doi.org/10.1371/journal.pone.0161930.

[48] Aurélie Goyenvalle et al., "Functional Correction in Mouse Models of Muscular Dystrophy Using Exon-Skipping Tricyclo-DNA Oligomers," *Nature Medicine* 21, no. 3 (March 2015): 270–75, https://doi.org/10.1038/nm.3765.

[49] Emily Linnane et al., "Differential Uptake, Kinetics and Mechanisms of Intracellular Trafficking of next-Generation Antisense Oligonucleotides across Human Cancer Cell Lines," *Nucleic Acids Research* 47, no. 9 (May 21, 2019): 4375–92, https://doi.org/10.1093/nar/gkz214.

[50] Anthony J. Snyder, Andrew T. Abad, and Pranav Danthi, "A CRISPR-Cas9 Screen Reveals a Role for WD Repeat-Containing Protein 81 (WDR81) in the Entry of Late Penetrating Viruses," *PLoS Pathogens* 18, no. 3 (March 2022): e1010398, https://doi.org/10.1371/journal.ppat.1010398.

[51] Mitsunori Fukuda, "Rab GTPases: Key Players in Melanosome Biogenesis, Transport, and Transfer," *Pigment Cell & Melanoma Research* 34, no. 2 (2021): 222–35, https://doi.org/10.1111/pcmr.12931.

[52] Sandra Kissing et al., "Vacuolar ATPase in Phagosome-Lysosome Fusion," *The Journal of Biological Chemistry* 290, no. 22 (May 29, 2015): 14166–80, https://doi.org/10.1074/jbc.M114.628891.

[53] Angeles García-Cazorla et al., "Genetic Disorders of Cellular Trafficking," *Trends in Genetics* 38, no. 7 (July 2022): 724–51, https://doi.org/10.1016/j.tig.2022.02.012.

Figure 1

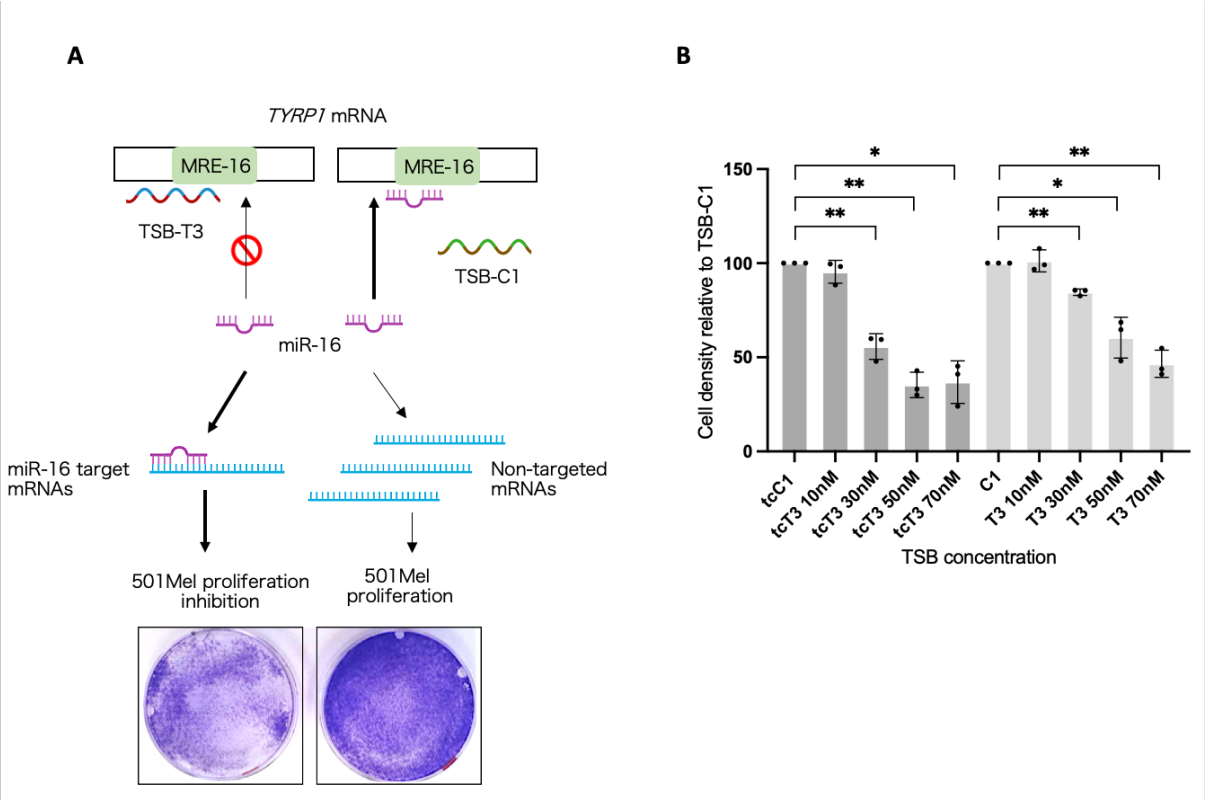
A
TYRP1 mRNA
MRE-16
MRE-16
TSB-T3
TSB-C1
miR-16
miR-16 target mRNAs
Non-targeted mRNAs
501Mel proliferation inhibition
501Mel proliferation
B
Cell density relative to TSB-C1
150
100
50
0
*
**
**
**
*
**
tcC1
tcT3 10nM
tcT3 30nM
tcT3 50nM
tcT3 70nM
C1
T3 10nM
T3 30nM
T3 50nM
T3 70nM
TSB concentration

Figure 2

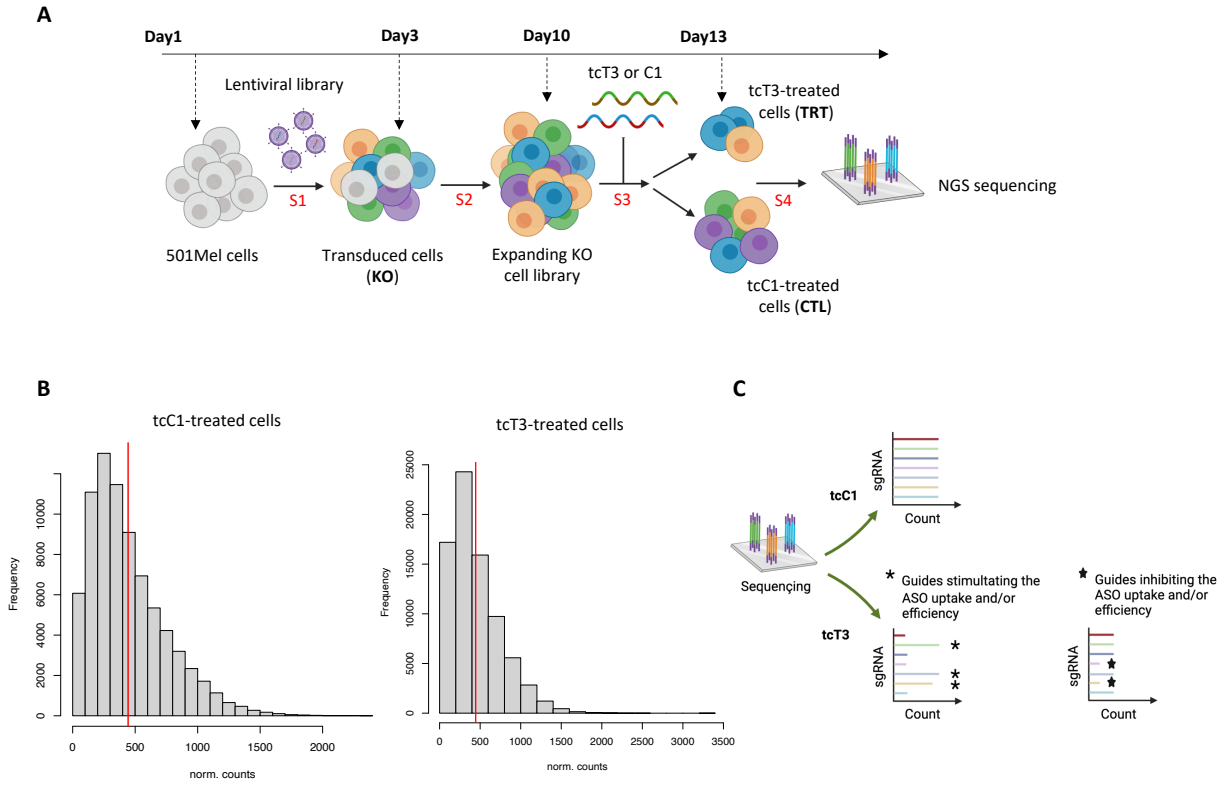
A
Day1
Day3
Day10
Day13
Lentiviral library
tcT3 or C1
tcT3-treated cells (TRT)
S1
S2
S3
S4
NGS sequencing
501Mel cells
Transduced cells (KO)
Expanding KO cell library
tcC1-treated cells (CTL)
B
tcC1-treated cells
tcT3-treated cells
Frequency
norm. counts
C
Sequençing
tcC1
tcT3
sgRNA
Count
Guides stimultating the ASO uptake and/or efficiency
Guides inhibiting the ASO uptake and/or efficiency

Figure 3

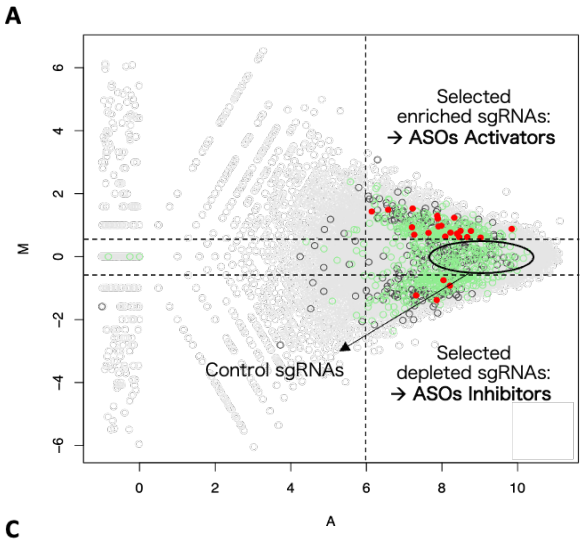

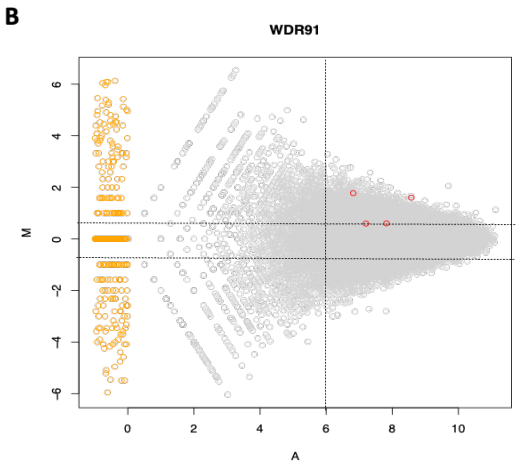

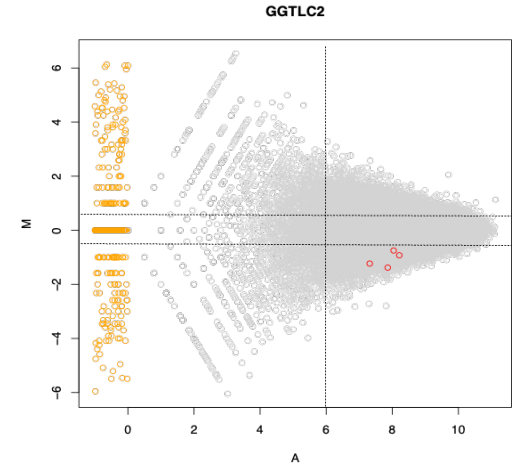

C

	Normalized Read counts		
sgRNA	CTL	TRT	Fold change
sgCOG8-1	110	204	1,854545455
sgCOG8-3	83	152	1,831325301
sgCOG8-4	85	165	1,941176471
sgWBSCR16-1	57	160	2,807017544
sgWBSCR16-2	107	204	1,906542056
sgWBSCR16-3	43	116	2,697674419
sgWBSCR16-4	156	360	2,307692308
sgWDR91-1	61	209	3,426229508
sgWDR91-3	219	664	3,03196347
sgGGTLC2-1	244	104	2,346153846
sgGGTLC2-2	375	144	2,604166667
sgGGTLC2-3	408	215	1,897674419
sgGGTLC2-4	341	203	1,679802956

Figure 4

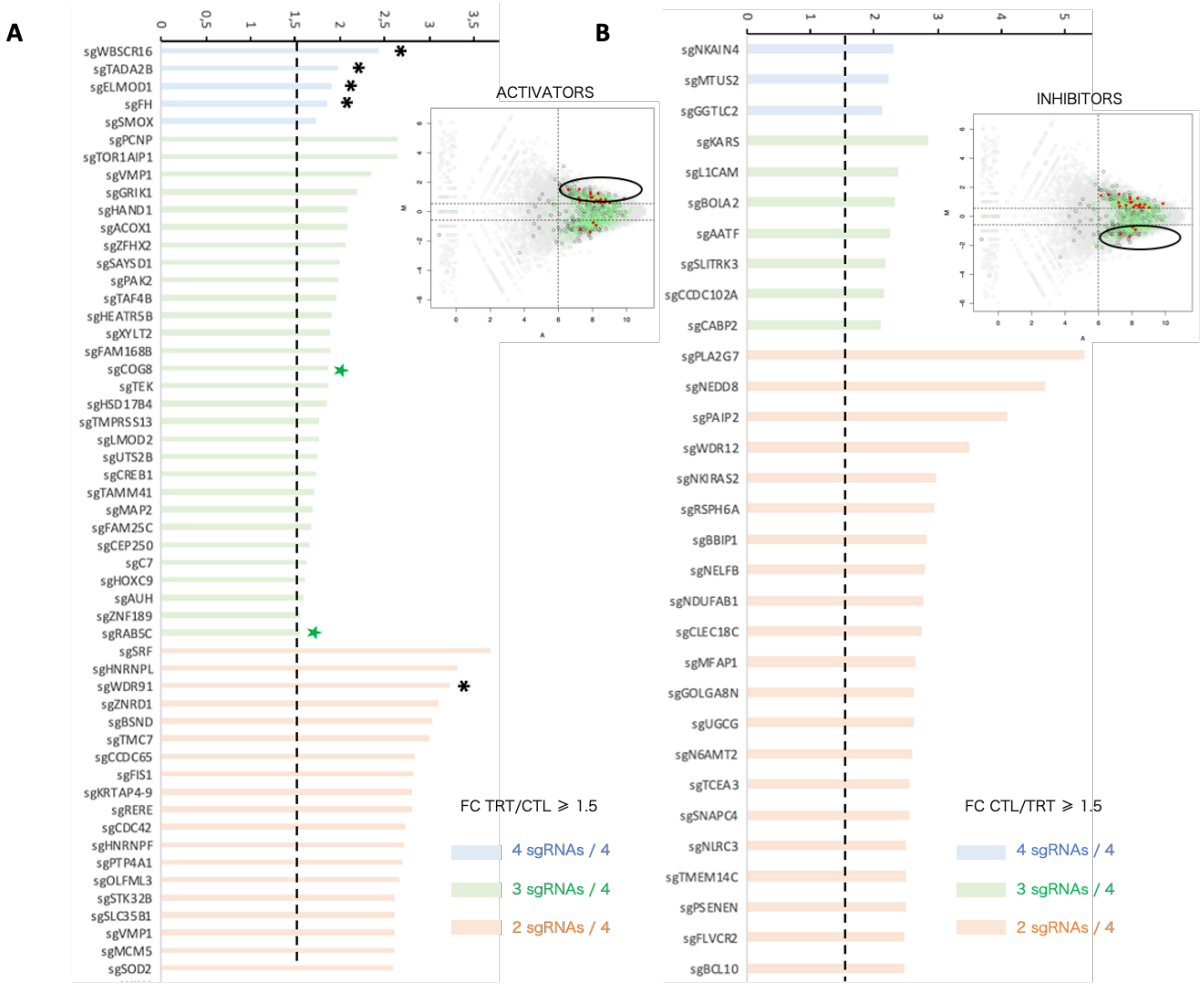
A
B
ACTIVATORS
INHIBITORS
FC TRT/CTL ⩾ 1.5
FC CTL/TRT ⩾ 1.5
4 sgRNAs / 4
3 sgRNAs / 4
2 sgRNAs / 4
sgWBSCR16
sgTADA2B
sgELMOD1
sgFH
sgSMOX
sgPCNP
sgTOR1AIP1
sgVMP1
sgGRIK1
sgHAND1
sgACOX1
sgZFHX2
sgSAYSD1
sgPAK2
sgTAF4B
sgHEATR5B
sgXYLT2
sgFAM168B
sgCOG8
sgTEK
sgHSD17B4
sgTMPRSS13
sgLMOD2
sgUTS2B
sgCREB1
sgTAMM41
sgMAP2
sgFAM25C
sgCEP250
sgC7
sgHOXC9
sgAUH
sgZNF189
sgRAB5C
sgSRF
sgHNRNPL
sgWDR91
sgZNRD1
sgBSND
sgTMC7
sgCCDC65
sgFIS1
sgKRTAP4-9
sgRERE
sgCDC42
sgHNRNPF
sgPTP4A1
sgOLFML3
sgSTK32B
sgSLC35B1
sgVMP1
sgMCM5
sgSOD2
sgNKAIN4
sgMTUS2
sgGGTLC2
sgKARS
sgL1CAM
sgBOLA2
sgAATF
sgSLITRK3
sgCCDC102A
sgCABP2
sgPLA2G7
sgNEDD8
sgPAIP2
sgWDR12
sgNKIRAS2
sgRSPH6A
sgBBIP1
sgNELFB
sgNDUFAB1
sgCLEC18C
sgMFAP1
sgGOLGA8N
sgUGCG
sgN6AMT2
sgTCEA3
sgSNAPC4
sgNLRC3
sgTMEM14C
sgPSENEN
sgFLVCR2
sgBCL10

Figure 5

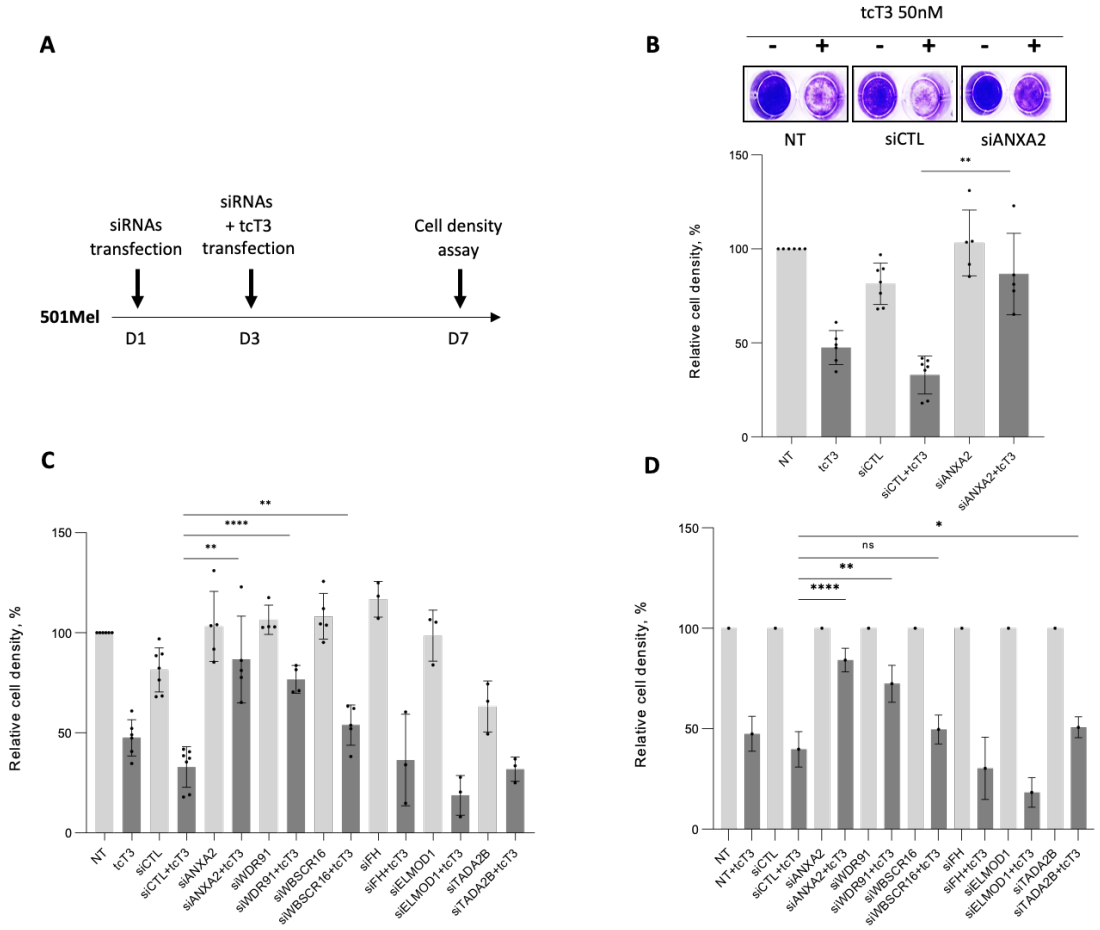
A
siRNAs transfection
siRNAs + tcT3 transfection
Cell density assay
501Mel
D1
D3
D7
B
tcT3 50nM
-
+
-
+
-
+
NT
siCTL
siANXA2
Relative cell density, %
150
100
50
0
**
NT
tcT3
siCTL
siCTL+tcT3
siANXA2
siANXA2+tcT3
C
Relative cell density, %
150
100
50
0
**
****
**
NT
tcT3
siCTL
siCTL+tcT3
siANXA2
siANXA2+tcT3
siWDR91
siWDR91+tcT3
siWBSCR16
siWBSCR16+tcT3
siFH
siFH+tcT3
siELMOD1
siELMOD1+tcT3
siTADA2B
siTADA2B+tcT3
D
Relative cell density, %
150
100
50
0
*
ns
**
****
NT
NT+tcT3
siCTL
siCTL+tcT3
siANXA2
siANXA2+tcT3
siWDR91
siWDR91+tcT3
siWBSCR16
siWBSCR16+tcT3
siFH
siFH+tcT3
siELMOD1
siELMOD1+tcT3
siTADA2B
siTADA2B+tcT3

Figure 6

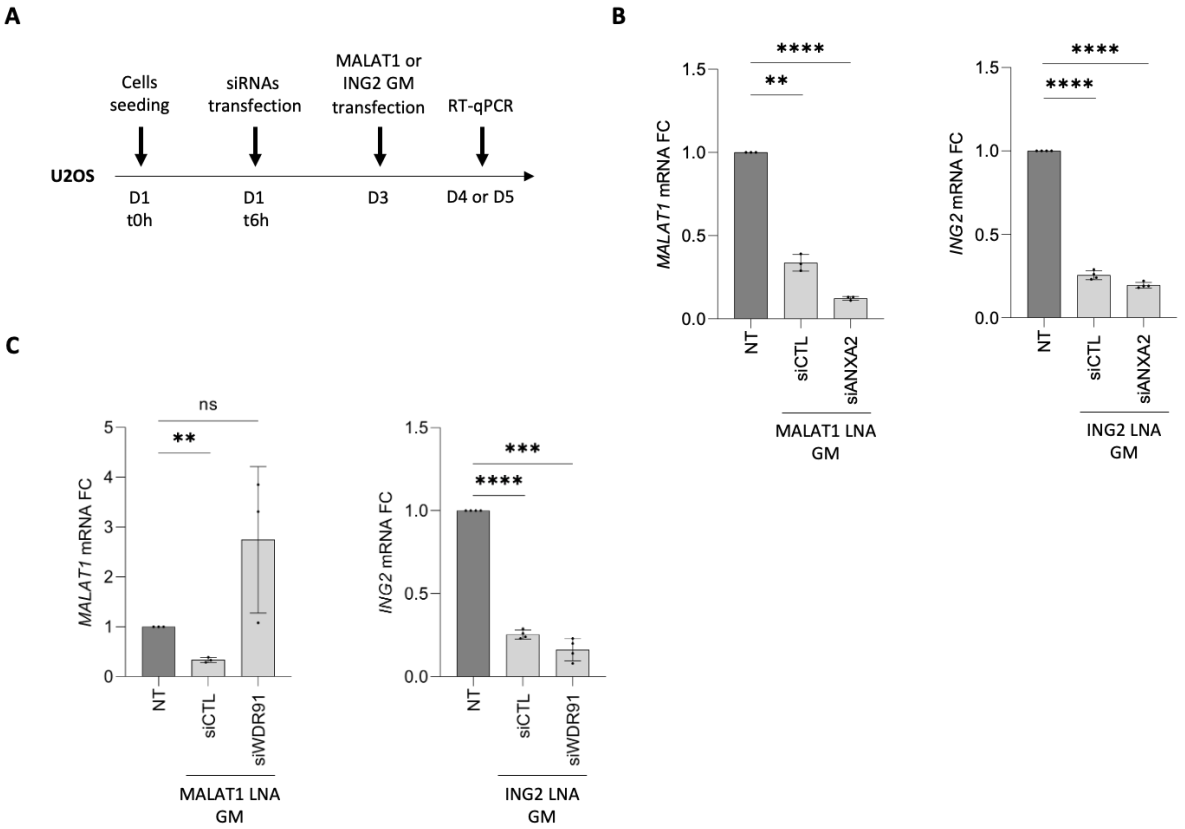
A
Cells seeding
siRNAs transfection
MALAT1 or ING2 GM transfection
RT-qPCR
U2OS
D1 t0h
D1 t6h
D3
D4 or D5
B
MALAT1 mRNA FC
ING2 mRNA FC
NT
siCTL
siANXA2
MALAT1 LNA GM
ING2 LNA GM
C
MALAT1 mRNA FC
ING2 mRNA FC
ns
siWDR91
MALAT1 LNA GM
ING2 LNA GM

Figure 7

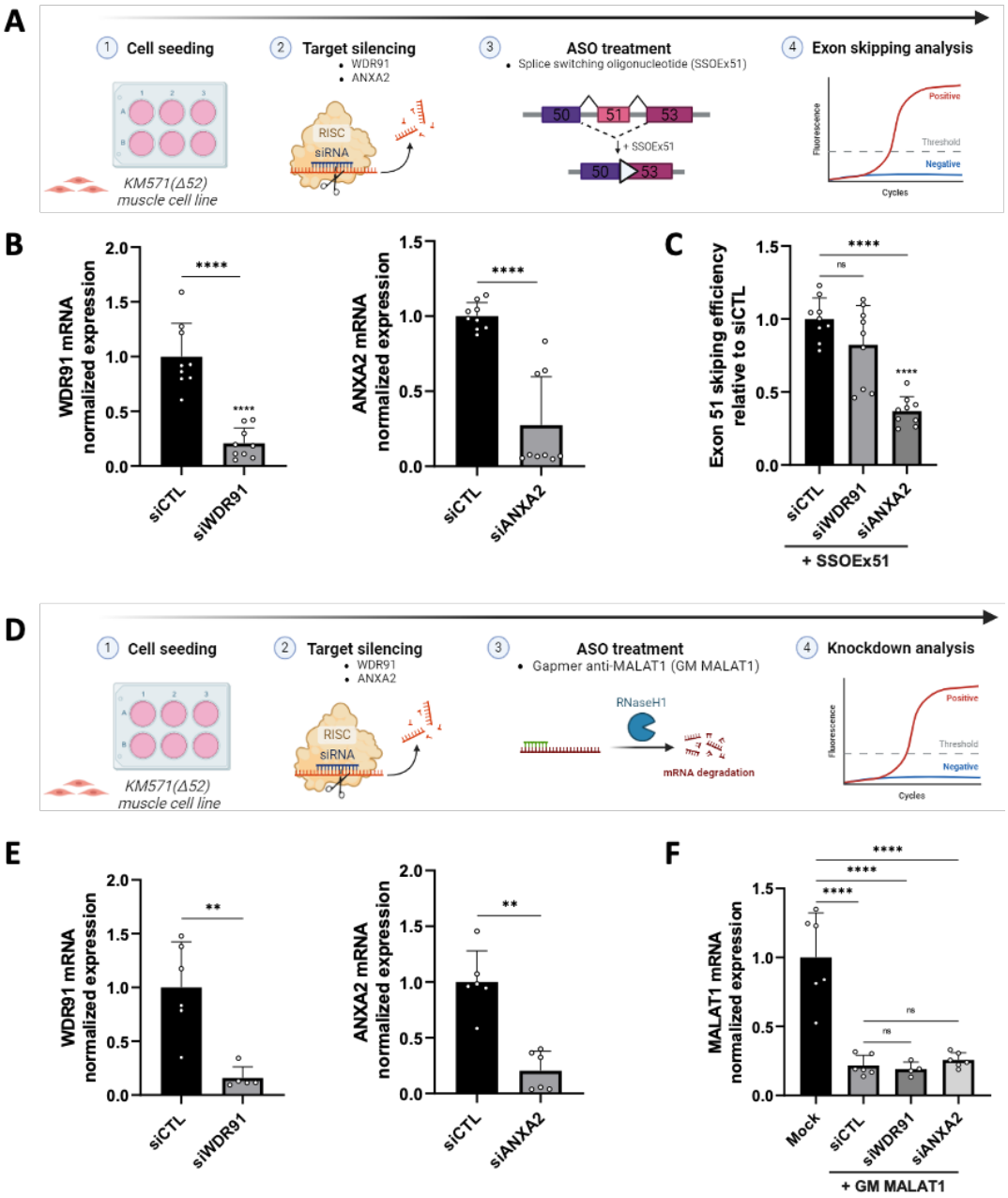
A
1 Cell seeding
KM571(Δ52) muscle cell line
2 Target silencing
WDR91
ANXA2
RISC
siRNA
3 ASO treatment
Splice switching oligonucleotide (SSOEx51)
50
51
53
+ SSOEx51
4 Exon skipping analysis
Fluorescence
Positive
Threshold
Negative
Cycles
B
WDR91 mRNA normalized expression
****
siCTL
siWDR91
ANXA2 mRNA normalized expression
siANXA2
C
Exon 51 skiping efficiency relative to siCTL
ns
+ SSOEx51
D
1 Cell seeding
KM571(Δ52) muscle cell line
2 Target silencing
WDR91
ANXA2
RISC
siRNA
3 ASO treatment
Gapmer anti-MALAT1 (GM MALAT1)
RNaseH1
mRNA degradation
4 Knockdown analysis
Fluorescence
Positive
Threshold
Negative
Cycles
E
WDR91 mRNA normalized expression
**
siCTL
siWDR91
ANXA2 mRNA normalized expression
siANXA2
F
MALAT1 mRNA normalized expression
Mock
siCTL
siWDR91
siANXA2
+ GM MALAT1